

Modeling and Correction of Pointing Errors in Gimbals-Type Optical Communication Terminals on Motion Platforms

Volume 13, Number 3, June 2021

Chao Peng
Dong He
Yuankang Wang
Yongmei Huang
Xiang Liu
Liangzhu Yuan
Yangjie Xu
Jiaming Lei
Haotong Ma



DOI: 10.1109/JPHOT.2021.3078227

Modeling and Correction of Pointing Errors in Gimbal-Type Optical Communication Terminals on Motion Platforms

Chao Peng ,^{1,2,3} Dong He,^{1,2,3} Yuankang Wang,^{1,2}
Yongmei Huang,^{1,2,3} Xiang Liu,^{1,2,3} Liangzhu Yuan,^{1,2,3}
Yangjie Xu,^{1,2,3} Jiaming Lei,^{1,2,3} and Haotong Ma ^{1,2,3}

¹Key Laboratory of Optical Engineering, Chinese Academy of Science,
Chengdu 610209, China

²Institute of Optics and Electronics, Chinese Academy of Science, Chengdu 610209, China

³University of Chinese Academy of Science, Beijing 100049, China

DOI:10.1109/JPHOT.2021.3078227

This work is licensed under a Creative Commons Attribution 4.0 License. For more information, see
<https://creativecommons.org/licenses/by/4.0/>

Manuscript received April 15, 2021; revised April 30, 2021; accepted May 3, 2021. Date of publication May 7, 2021; date of current version June 1, 2021. This work was supported by the National Natural Science Foundation of China under Grant 2019JDJQ0012. Corresponding authors: Dong He; Yongmei Huang (e-mail: hedong@ioe.ac.cn; huangym@ioe.ac.cn).

Abstract: In free-space optical (FSO) communication, high-precision pointing is a critical technology required for rapid acquisition to reduce link establishment time and increase communication time. FSO communication on a motion platform is necessary to expand the communication area and to promote the establishment of a global communication network. However, the pointing accuracy of an optical communication terminal on a motion platform is low due to numerous error sources and error coupling. This paper evaluates the error sources and proposes a pointing model to avoid problems resulting from error coupling. This proposed pointing model was designed to improve the pointing accuracy of a gimbal-type optical communication terminal (GOCT) on a motion platform. The effectiveness of the proposed pointing model was verified by tracking star experiments. The modified residual error of the proposed point model was 94.8 μ rad compared to 1324.2 μ rad without correction. Additionally, the modified residual error was 94.8 μ rad of the proposed pointing model compared to 140.2 μ rad of the existing model. The actual open-loop pointing error was reduced from 150.4 μ rad of the existing model to 101.3 μ rad of the proposed model. Thus, the pointing accuracy of a GOCT on a motion platform was significantly improved after correction by the proposed pointing model.

Index Terms: FSO communication, GOCT, motion platform, pointing error analysis, pointing model.

1. Introduction

Free-space optical (FSO) communication is widely used in the communication field due to its superior performance. A gimbal-type optical communication terminal (GOCT) is the most common communication terminal in FSO communication. A GOCT has an extensive tracking range and is easy to control. Laser communication technology is evolving from a fixed platform to a motion platform to meet global communication networking needs. The laser beams are very narrow in long-distance point-to-point laser communication. Thus, high-precision pointing systems are

required to ensure the rapid acquisition of the two communication terminals with high probability. The rapid acquisition of the two communication terminals reduces the link establishment time and increases the communication time. However, the pointing accuracy of a GOCT on a motion platform is low due to numerous error sources and error coupling. Reducing pointing errors by using high-precision devices and mechanical manufacturing processes is costly. Thus, it is necessary to model and correct the pointing errors of a GOCT on a motion platform.

The design of a pointing system for a GOCT on a motion platform is based on research on the pointing systems for GOCTs on fixed platforms. Previous research reports good correction results for the pointing systems of GOCTs on fixed platforms. Geometric and nonlinear errors are the main pointing error sources for GOCTs on fixed platforms. He *et al.* [1] used a mount model to correct a telescope's geometric errors in satellite–ground quantum experiments. Yan *et al.* [2] used an Allan variance based semi-parameter model to correct pointing errors in alt-az telescopes. Huang *et al.* [3] analyzed the errors from a telescope's kinematics using a semi-parametric regression model to eliminate the geometric and nonlinear errors. Tang *et al.* [4] analyzed geometric error sources using quaternions. They proposed a semi-parametric model based on a least square collocation method. Fisk *et al.* [5] studied the pointing system of a gimbaled inertial stabilized platform and employed a physical mathematical model to address the geometric errors. Wu *et al.* [6] modeled the pointing error angles in periscope-type optical communication terminals. Luck [7] investigated mount model stability as a technique for maintaining high-precision pointing for an extended length of time.

Unlike a fixed platform, a motion platform is equipped with an attitude sensor. However, the attitude sensors introduce attitude errors and installation errors. Shim *et al.* [8] and Epple [9] used a strap-down initial navigation system (INS) in combination with a global positioning system (GPS) as the initial pointing system sensor for achieving the initial pointing for a line of sight (LOS). Wu *et al.* [10] introduced an extended Kalman filtering technique into attitude estimation to improve pointing accuracy in airship–ship and aircraft–aircraft experiments. Zhao *et al.* [11] used a LOS calibration method to improve the performance of the pointing system in a short-distance aircraft laser communication demonstration experiment. Shrestha *et al.* [12] used a tracking star method to improve pointing accuracy. However, this study did not provide a calibration model.

There are more pointing error sources for a GOCT on a motion platform than for a GOCT on a fixed platform. However, the cited literature does not include the entire error sources when calibrating pointing errors. He *et al.* [13] evaluated simultaneous installation errors and geometric errors. They used the least square method twice to estimate the installation errors and geometric errors, respectively. Their method has the problem of coupling of error parameter calculations because the error parameters are not calculated simultaneously. Also, most of the literature investigated short-distance pointing, which is simpler than long-distance pointing. The laser divergence angle can be increased in short-distance pointing to reduce the pointing precision requirements. In this paper, we propose a pointing model to improve the pointing accuracy of a GOCT on a motion platform for long-distance FSO communication. The proposed model not only simultaneously considers attitude errors, installation errors, and geometric errors, but also avoids the influence of error coupling. The proposed model was verified by tracking star experiments. The experimental results showed that the pointing accuracy of a GOCT on a motion platform was significantly improved after correction by the proposed pointing model.

2. Error Sources Analysis and Modeling

2.1 Error Sources Analysis

The structure of a GOCT is shown in Fig. 1. The LOS points to a target by rotation of the azimuth axis and elevation axis. High-precision pointing is required for rapid acquisition before starting FSO communication. However, the LOS cannot accurately point to the target due to attitude errors, installation errors, and geometric errors. Pointing error is defined as the difference between the actual direction and the ideal direction. As shown in Fig. 2 [3], the vector of pointing errors is given

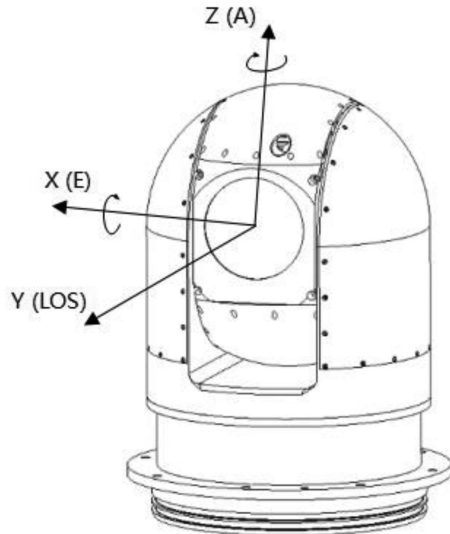


Fig. 1. Structure of the GOCT.

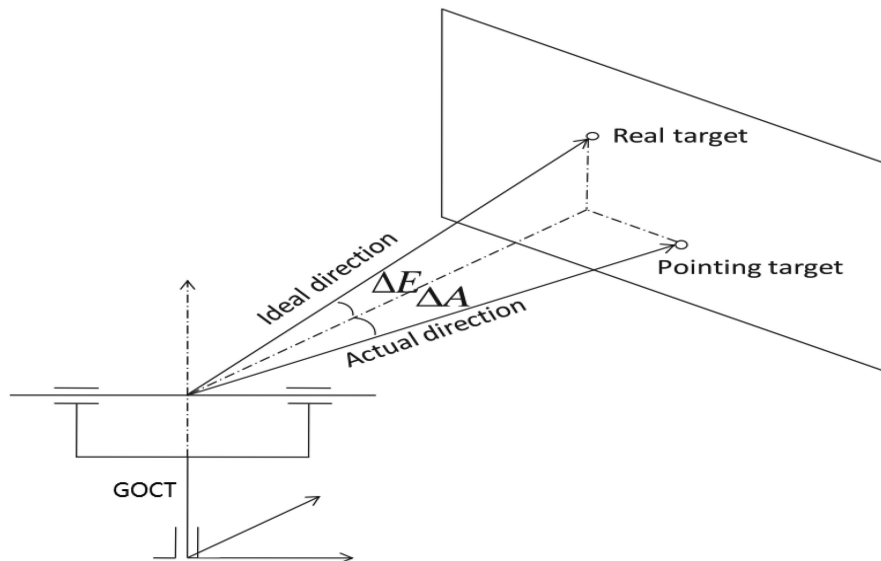


Fig. 2. Pointing errors of the GOCT [3].

by $\Delta = [\Delta A, \Delta E]^T$. The pointing errors are defined by Equation (1):

$$\begin{cases} \Delta A = A - \hat{A} \\ \Delta E = E - \hat{E} \end{cases} \quad (1)$$

where ΔA is the pointing error of the azimuth axis, and ΔE is the pointing error of the elevation axis. A and E are the encoder measurement values of the azimuth axis and elevation axis, respectively, when the target is imaged at the center of a charge-coupled device (CCD). \hat{A} and \hat{E} are the encoder guide values for the azimuth axis and elevation axis, respectively. The target position, device attitude, and pointing error compensation are used to calculate the encoder guide values.

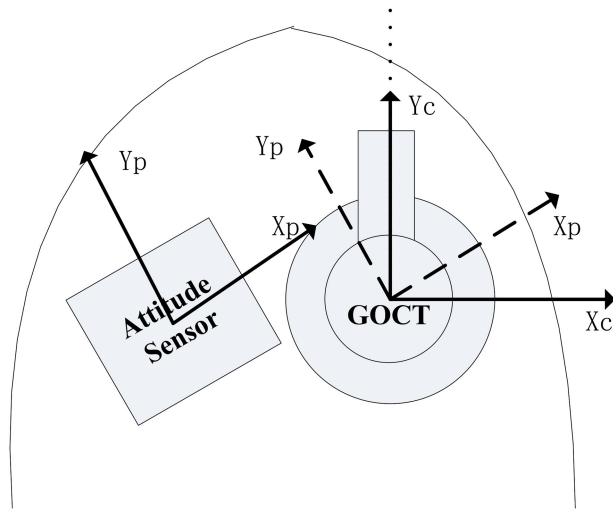


Fig. 3. Installation errors between the GOCT and attitude sensor [13].

ΔA and ΔE must be reduced to reduce the pointing error. Thus, the encoder guide values (i.e., \hat{A} and \hat{E}) must be closer to their respective encoder measurement values (i.e., A and E).

Attitude errors, installation errors, and geometric errors are the primary pointing error sources for a GOCT on a motion platform. Attitude errors occur when an attitude sensor inaccurately measures its own attitude. Installation errors refer to the installation deviation between an attitude sensor and the GOCT device. Installation errors cause a deviation angle between the measuring axis of the attitude sensor and the GOCT pointing axis. Installation errors are illustrated in Fig. 3 [13]. Geometric errors occur during the manufacturing, assembly, installation, and operation of a GOCT. Geometric errors include azimuth and elevation bearing errors, azimuth and elevation encoder errors, non-orthogonality of the azimuth and elevation axis, and misalignment of the optical axis and tube flexure. The azimuth and elevation bearing errors are caused by the radial runout of the azimuth and elevation axis during rotation. The azimuth and elevation encoder errors refer to the measurement errors of the rotation angles of the azimuth and elevation axis. The misalignment of the optical axis is caused by the optical axis not being perpendicular to the azimuth and elevation axis. The tube flexure mainly refers to the deformation of the tube caused by gravity, which makes the LOS point to a lower elevation.

2.2 Error Sources Modeling

The Denavit–Hartenberg (D-H) convention [14] was used to model error sources. In the D-H convention, each error source is represented by a 4 by 4 matrix. This matrix represents the rotation and translation of the LOS. Rotation is important, and translation is usually small with a negligible effect on pointing for long-distance in a GOCT [14]. Therefore, the rotation-only D-H convention was selected to model error sources. In this study, each error source was represented by a 3 by 3 rotation matrix.

In this study, the rotation matrix was divided into two types: a rotation matrix representing the rotation of the coordinate system and a rotation matrix representing the rotation of a vector in the coordinate system. The rotation angle is also directional. In the commonly used GOCT system on a motion platform, the attitude sensor measures the rotation Euler angle of its own coordinate system relative to the Northeast celestial coordinate system. This includes the yaw angle H rotating around the z -axis, the pitch angle P rotating around the x -axis, and the roll angle R rotating around the y -axis. Looking against the rotation axis direction, H is positive when rotating clockwise, while P and R are positive when rotating counterclockwise. When the azimuth and elevation encoders

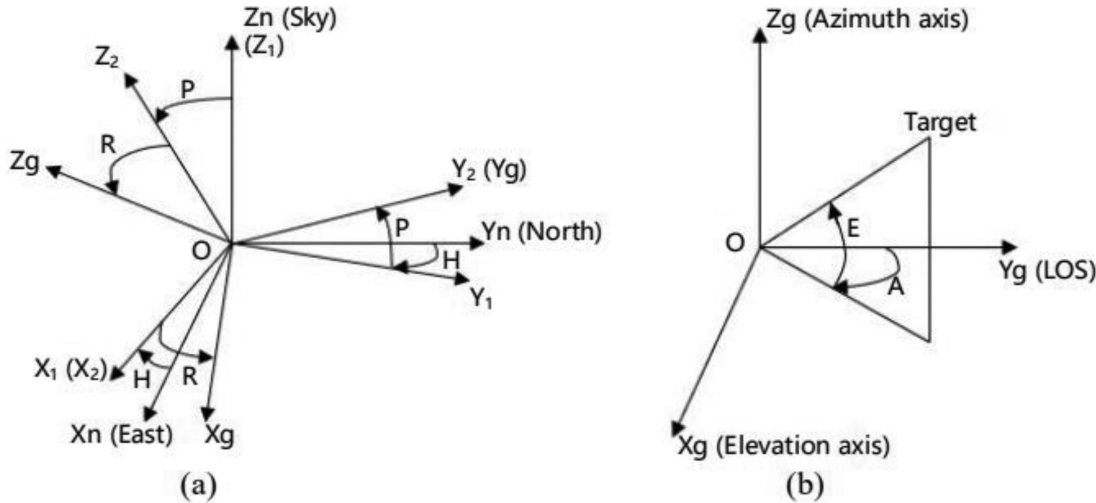


Fig. 4. Schematic diagram of the coordinate system of a GOCT on a motion platform.

are 0, the elevation axis, LOS, and azimuth axis of the GOCT are aligned with the x-axis, y-axis, and z-axis of the attitude sensor, respectively. The rotation range of the azimuth axis is $0 \sim 360^\circ$, and the encoder value A is positive when the GOCT rotates clockwise. The rotation range of the elevation axis is $0 \sim 90^\circ$, and the encoder value E is positive when the LOS moves upward. The coordinate system of a GOCT on a motion platform is shown in Fig. 4. O-XnYnZn represents the Northeast celestial coordinate system, and O-XgYgZg represents the attitude sensor coordinate system. The O-XnYnZn coincides with the O-XgYgZg after successive yaw, pitch, and roll rotations. To correspond with the commonly used GOCT system on a motion platform, we define the rotation matrix of the coordinate system rotation by Equation (2):

$$R_{x1} = \begin{bmatrix} 1 & 0 & 0 \\ 0 & \cos \theta & \sin \theta \\ 0 & -\sin \theta & \cos \theta \end{bmatrix}, \quad R_{y1} = \begin{bmatrix} \cos \theta & 0 & -\sin \theta \\ 0 & 1 & 0 \\ \sin \theta & 0 & \cos \theta \end{bmatrix}, \quad R_{z1} = \begin{bmatrix} \cos \theta & -\sin \theta & 0 \\ \sin \theta & \cos \theta & 0 \\ 0 & 0 & 1 \end{bmatrix} \quad (2)$$

The rotation matrix of the vector rotation in the coordinate system is defined by Equation (3):

$$R_{x2} = \begin{bmatrix} 1 & 0 & 0 \\ 0 & \cos \theta & -\sin \theta \\ 0 & \sin \theta & \cos \theta \end{bmatrix}, \quad R_{y2} = \begin{bmatrix} \cos \theta & 0 & -\sin \theta \\ 0 & 1 & 0 \\ \sin \theta & 0 & \cos \theta \end{bmatrix}, \quad R_{z2} = \begin{bmatrix} \cos \theta & \sin \theta & 0 \\ -\sin \theta & \cos \theta & 0 \\ 0 & 0 & 1 \end{bmatrix}. \quad (3)$$

where R_{x1} , R_{y1} , and R_{z1} represent the rotation of the coordinate system around the x-axis, y-axis, and z-axis, respectively. R_{x2} , R_{y2} , and R_{z2} represent the rotation of the vector around the x-axis, y-axis, and z-axis, respectively.

Based on the coordinate system and rotation matrix definitions, we summarize the error sources in Table 1. The symbols represent the error angles of the error sources. The use of some symbols refers to the reference [14]. Rotation type 1 represents the rotation of the coordinate system, and rotation type 2 represents the rotation of the vector in the coordinate system. The matrix of each error source needs to be calculated. A small angle approximation is applied during calculation because each error angle is very small [15]. For a small angle Δ , we have $\sin \Delta \approx \Delta$, $\cos \Delta \approx 1$ and $\Delta \cdot \Delta \approx 0$. Additionally, each rotation matrix is an orthogonal matrix that satisfies $R^{-1} = R^T$.

The attitude errors include the yaw angle error ΔH , pitch angle error ΔP , and roll angle error ΔR . We denote the yaw, pitch, and roll attitude matrices measured by the attitude sensor as R_h , R_p and

TABLE 1
Summary of Error Sources

Error sources	Symbol	Matrix	Rotation axis	Rotation type
Attitude errors	$\Delta H, \Delta P, \Delta R$	R_c	—	1
Installation errors	$\alpha_1, \alpha_2, \alpha_3$	R_φ	—	1
Azimuth encoder errors	$A, A_{\beta 1}, A_{\beta 2}$	R_A	Z	2
Elevation encoder errors	$E, E_{\beta 1}, E_{\beta 2}$	R_E	X	2
Optical axis tilts toward z-axis	γ_x	R_{Mx}	X	2
Optical axis tilts toward x-axis	γ_z	R_{Mz}	Z	2
Tube flexure	$\delta_T \cot E$	R_F	X	2
Non-orthogonality of azimuth and elevation axis	η	R_N	Y	2
Elevation bearing tilts toward z-axis	$\xi_{B1} \cos E$	R_{B1}	Y	2
Elevation bearing tilts toward y-axis	$\xi_{B2} \cos E$	R_{B2}	Z	1
Azimuth bearing tilts toward y-axis	$\xi_{B3} \cos A$	R_{B3}	X	1
Azimuth bearing tilts toward x-axis	$\xi_{B4} \cos A$	R_{B4}	Y	1

R_r , respectively. The attitude matrices R_h , R_p and R_r are given by Equation (4):

$$R_h = \begin{bmatrix} \cos H & -\sin H & \cos H & 0 \\ 0 & 0 & 1 & 0 \end{bmatrix}, R_p = \begin{bmatrix} 1 & 0 & 0 \\ 0 & \cos P & \sin P \\ 0 & -\sin P & \cos P \end{bmatrix}, R_r = \begin{bmatrix} \cos R & 0 & -\sin R \\ 0 & 1 & 0 \\ \sin R & 0 & \cos R \end{bmatrix} \quad (4)$$

The corresponding attitude error matrices $R_{\Delta h}$, $R_{\Delta p}$ and $R_{\Delta r}$ are given by Equation (5):

$$R_{\Delta h} \approx \begin{bmatrix} 1 & -\Delta H & 0 \\ \Delta H & 1 & 0 \\ 0 & 0 & 1 \end{bmatrix}, R_{\Delta p} \approx \begin{bmatrix} 1 & 0 & 0 \\ 0 & 1 & \Delta P \\ 0 & -\Delta P & 1 \end{bmatrix}, R_{\Delta r} \approx \begin{bmatrix} 1 & 0 & -\Delta R \\ 0 & 1 & 0 \\ \Delta R & 0 & 1 \end{bmatrix} \quad (5)$$

R_c is used to correct the three attitude angle errors. Therefore, we derive Equation (6):

$$R_{\Delta r} R_r R_{\Delta p} R_p R_{\Delta h} R_h = R_c R_r R_p R_h \quad (6)$$

Transforming Equation (6), we get Equation (7):

$$R_c = R_{\Delta r} R_r R_{\Delta p} R_p R_{\Delta h} R_p^T R_r^T$$

$$\approx \begin{bmatrix} 1 & \Delta P \sin R - \Delta H \cos R \cos P & -\Delta R + \Delta H \sin P \\ -\Delta P \sin R + \Delta H \cos R \cos P & 1 & \Delta P \cos R + \Delta H \sin R \cos P \\ \Delta R - \Delta H \sin P & -\Delta P \cos R - \Delta H \sin R \cos P & 1 \end{bmatrix} \quad (7)$$

The installation errors include three error angles α_1 , α_2 , and α_3 . Rotating the coordinate system of the attitude sensor around the z-axis, x-axis, and y-axis by the α_3 , α_2 , and α_1 angles, respectively, can eliminate the installation errors. The installation error matrix R_φ is given by Equation (8):

$$R_\varphi \approx \begin{bmatrix} 1 & 0 & -\alpha_1 \\ 0 & 1 & 0 \\ \alpha_1 & 0 & 1 \end{bmatrix} \begin{bmatrix} 1 & 0 & 0 \\ 0 & 1 & \alpha_2 \\ 0 & -\alpha_2 & 1 \end{bmatrix} \begin{bmatrix} 1 & -\alpha_3 & 0 \\ \alpha_3 & 1 & 0 \\ 0 & 0 & 1 \end{bmatrix} \approx \begin{bmatrix} 1 & -\alpha_3 & -\alpha_1 \\ \alpha_3 & 1 & \alpha_2 \\ \alpha_1 & -\alpha_2 & 1 \end{bmatrix} \quad (8)$$

The encoder errors include encoder offset, scale error, and eccentricity error. The offset errors of the azimuth and elevation encoder are denoted by $A_{\beta 1}$ and $E_{\beta 1}$, respectively. The scale errors of the azimuth and elevation encoder are expressed as $m_1 A / 2\pi$ and $n_1 E / 2\pi$, respectively [7], [16]. The eccentricity error of the azimuth encoder is expressed by $m_2 \sin A$ and $m_3 \cos A$. The eccentricity error of the elevation encoder is expressed by $n_2 \sin E$ and $n_3 \cos E$ [16]. A and E are the azimuth and elevation encoder values, respectively. We use $A_{\beta 2}$ to represent the sum of scale error and eccentricity error of the azimuth encoder (Eq. 9). We use $E_{\beta 2}$ to represent the sum of scale error and eccentricity error of the elevation encoder (Eq. 10).

$$A_{\beta 2} = m_1 A / 2\pi + m_2 \sin A + m_3 \cos A \quad (9)$$

$$E_{\beta 2} = n_1 E / 2\pi + n_2 \sin E + n_3 \cos E \quad (10)$$

Therefore, the actual rotation angles of the LOS around the azimuth and elevation axis are $A + A_{\beta 1} + A_{\beta 2}$ and $E + E_{\beta 1} + E_{\beta 2}$, respectively. The azimuth rotation matrix R_A is given by Equation (11):

$$R_A = \begin{bmatrix} \cos(A + A_{\beta 1} + A_{\beta 2}) & \sin(A + A_{\beta 1} + A_{\beta 2}) & 0 \\ -\sin(A + A_{\beta 1} + A_{\beta 2}) & \cos(A + A_{\beta 1} + A_{\beta 2}) & 0 \\ 0 & 0 & 1 \end{bmatrix}$$

$$\approx \begin{bmatrix} 1 & A_{\beta 1} & 0 \\ -A_{\beta 1} & 1 & 0 \\ 0 & 0 & 1 \end{bmatrix} \begin{bmatrix} \cos A - A_{\beta 2} \sin A & \sin A + A_{\beta 2} \cos A & 0 \\ -\sin A - A_{\beta 2} \cos A & \cos A - A_{\beta 2} \sin A & 0 \\ 0 & 0 & 1 \end{bmatrix} \quad (11)$$

Which is separated into Equation (12):

$$R_{A\beta 1} = \begin{bmatrix} 1 & A_{\beta 1} & 0 \\ -A_{\beta 1} & 1 & 0 \\ 0 & 0 & 1 \end{bmatrix}, \quad R_{A\beta 2} = \begin{bmatrix} \cos A - A_{\beta 2} \sin A & \sin A + A_{\beta 2} \cos A & 0 \\ -\sin A - A_{\beta 2} \cos A & \cos A - A_{\beta 2} \sin A & 0 \\ 0 & 0 & 1 \end{bmatrix} \quad (12)$$

Thus, Equation (13) is determined:

$$R_A \approx R_{A\beta 1} R_{A\beta 2} \quad (13)$$

The elevation rotation matrix R_E is given by Equation (14):

$$R_E = \begin{bmatrix} 1 & 0 & 0 \\ 0 & \cos(E + E_{\beta 1} + E_{\beta 2}) & -\sin(E + E_{\beta 1} + E_{\beta 2}) \\ 0 & \sin(E + E_{\beta 1} + E_{\beta 2}) & \cos(E + E_{\beta 1} + E_{\beta 2}) \end{bmatrix}$$

$$\approx \begin{bmatrix} 1 & 0 & 0 \\ 0 & \cos E - (E_{\beta 1} + E_{\beta 2}) \sin E & -\sin E - (E_{\beta 1} + E_{\beta 2}) \cos E \\ 0 & \sin E + (E_{\beta 1} + E_{\beta 2}) \cos E & \cos E - (E_{\beta 1} + E_{\beta 2}) \sin E \end{bmatrix} \quad (14)$$

The remaining errors are geometric errors. The misalignment of the optical axis, the azimuth bearing error, and the elevation bearing error are divided into two corresponding tilt items, as shown in Table 1. The tube flexure, the azimuth bearing error, and the elevation bearing error are dynamic errors. These error angles can be expressed as a function of azimuth or elevation angle [14]. For example, the tube flexure can be expressed as $\delta_T \cot E$. The error matrix results from the substitution of the error angle symbol into the rotation matrix and is based on the rotation axis and rotation type. For example, substituting $\delta_T \cot E$ into R_{x2} for the tube flexure results in Equation (15):

$$R_F = \begin{bmatrix} 1 & 0 & 0 \\ 0 & \cos(\delta_T \cot E) & -\sin(\delta_T \cot E) \\ 0 & \sin(\delta_T \cot E) & \cos(\delta_T \cot E) \end{bmatrix} \approx \begin{bmatrix} 1 & 0 & 0 \\ 0 & 1 & -\delta_T \cot E \\ 0 & \delta_T \cot E & 1 \end{bmatrix} \quad (15)$$

The matrix models of all error sources are now determined.

3. Pointing Model Derivation

The proposed pointing model consists of an error parameter calculation model and a guide value calculation model. The error parameter calculation model calculates the value of each error source. The guide value calculation model calculates the guide value of the encoder for pointing.

3.1 The Error Parameter Calculation Model

The location of the target is known in the pointing process. The position angles A_n and E_n of the target are located in the Northeast celestial coordinate system of the GOCT location. The unit direction vector $(x_n, y_n, z_n)^T$ of the target in the Northeast celestial coordinate system is determined based on the position angles, as shown in Equation (16):

$$\begin{cases} x_n = \cos E_n \sin A_n \\ y_n = \cos E_n \cos A_n \\ z_n = \sin E_n \end{cases} \quad (16)$$

Then, the unit direction vector $(x_g, y_g, z_g)^T$ of the target in the attitude sensor coordinate system is determined using attitude information from the attitude sensor, as shown in Equation (17):

$$(x_g, y_g, z_g)^T = R_r R_p R_h (x_n, y_n, z_n)^T \quad (17)$$

Next, the order of rotation represented by each error matrix of rotation type 1 is determined by multiplying the relevant matrices by $(x_g, y_g, z_g)^T$, as shown in Equation (18). This calculation determined the direction vector $(x_t, y_t, z_t)^T$ of the target in the GOCT body coordinate system. The body coordinate system refers to the coordinate system determined by the current position of the GOCT after the generation of these error sources. Equation (18) assumes that the GOCT only has rotation type 1 error sources:

$$(x_t, y_t, z_t)^T = R_{B2} R_{B3} R_{B4} R_\varphi R_c (x_g, y_g, z_g)^T \quad (18)$$

The rotation type 2 error source affects the LOS position vector in the body coordinate system. The position vector of the LOS is $(0, 1, 0)^T$ without these errors. The optical axis tilting toward the x-axis and z-axis and the tube flexure only affect the position of the LOS. The non-orthogonality of the azimuth and elevation axis and the elevation bearing tilting toward the z-axis cause the LOS and the elevation axis to rotate around the y-axis simultaneously. Consequently, the LOS and the elevation axis deviate from their ideal positions. Therefore, the LOS rotates around a non-ideal elevation axis

in the actual rotation. However, the LOS is first rotated around the ideal elevation axis and then around the y-axis in the calculation. This calculation has the same effect as the actual rotation. Additionally, the elevation rotation needs to be performed before the azimuth rotation because the azimuth rotation changes the position of the elevation axis. The position vector $(x_s, y_s, z_s)^T$ of the LOS in the GOCT body coordinate system after the rotation of azimuth and elevation axis is expressed by Equation (19):

$$(x_s, y_s, z_s)^T = R_A R_N R_{B1} R_E R_F R_{Mx} R_{Mz} (0, 1, 0)^T \quad (19)$$

The LOS points to the target after the azimuth and elevation rotation, as expressed by Equation (20):

$$(x_t, y_t, z_t)^T = (x_s, y_s, z_s)^T \quad (20)$$

Equation (18) and Equation (19) are substituted into Equation (20) to produce Equation (21):

$$R_{B2} R_{B3} R_{B4} R_\varphi R_c (x_g, y_g, z_g)^T = R_A R_N R_{B1} R_E R_F R_{Mx} R_{Mz} (0, 1, 0)^T \quad (21)$$

Next, Equation (13) is substituted into Equation (21). Using the properties of an orthogonal matrix and after determining that the matrix multiplication is commutative, Equation (22) is obtained:

$$R_{A\beta 1}^T R_\varphi R_c (x_g, y_g, z_g)^T = R_{B4}^T R_{B3}^T R_{B2}^T R_{A\beta 2} R_N R_{B1} R_E R_F R_{Mx} R_{Mz} (0, 1, 0)^T \quad (22)$$

Substituting the expression of each error matrix into Equation (22) yields Equation (23):

$$(x_z, y_z, z_z)^T = B \cdot \vec{c} \quad (23)$$

where $(x_z, y_z, z_z)^T = (x_g - \sin A \cos E, y_g - \cos A \cos E, z_g - \sin E)^T$,

$$B = \begin{bmatrix} z_g & 0 & -x_g \\ -y_g \sin R & x_g \sin R - z_g \cos R & y_g \cos R \\ y_g \cos R \cos P - z_g \sin P & -x_g \cos R \cos P - z_g \sin R \cos P & x_g \sin P + y_g \sin R \cos P \\ 0 & -z_g & y_g \\ y_g & -x_g & 0 \\ -\sin A \sin E & -\cos A \sin E & \cos E \\ \cos A & -\sin A & 0 \\ -\sin A \cos E & -\cos A \cos E & \cos E \cot E \\ -\cos A \sin E & \sin A \sin E & 0 \\ -\cos A \sin E \cos E & \sin A \sin E \cos E & 0 \\ \cos A \cos^2 E & -\sin A \cos^2 E & 0 \\ 0 & -\cos A \sin E & \cos^2 A \cos E \\ \cos A \sin E & 0 & -\sin A \cos A \cos E \\ A \cos A \cos E / 2\pi & -A \sin A \cos E / 2\pi & 0 \\ \sin A \cos A \cos E & -\sin^2 A \cos E & 0 \\ \cos^2 A \cos E & -\sin A \cos A \cos E & 0 \\ -E \sin A \sin E / 2\pi & -E \cos A \sin E / 2\pi & E \cos E / 2\pi \\ -\sin A \sin^2 E & -\cos A \sin^2 E & \sin E \cos E \\ -\sin A \sin E \cos E & -\cos A \sin E \cos E & \cos^2 E \end{bmatrix}^T$$

\vec{c} is the error parameter vector:

$$\vec{c} = [\Delta R + \alpha_1, \Delta P, \Delta H, \alpha_2, \alpha_3 + A_{\beta 1}, E_{\beta 1} + \gamma_x, \gamma_z, \delta_T, \eta, \xi_{B1}, \xi_{B2}, \xi_{B3}, \xi_{B4}, m_1, m_2, m_3, n_1, n_2, n_3]^T.$$

The error parameter vector \vec{c} in Equation (23) is estimated using the least square method, as expressed in Equation (24):

$$\vec{c} = (B^T B)^{-1} B^T (x_z, y_z, z_z)^T \quad (24)$$

The error parameter calculation model is now complete. The error parameter calculation model is comprised of Equations (16), (17), and (23). The least square method is used to estimate the error parameters. The coupling of error parameter calculations is minimized because all parameters are calculated simultaneously. Coupled error parameters in \vec{c} still exist, including parameters $\Delta R + \alpha_1$, $\alpha_3 + A_{\beta 1}$, and $E_{\beta 1} + \gamma_x$. However, these coupled error parameters do not influence the guide value calculation.

3.2 The Guide Value Calculation Model

After determining the error parameters, the encoder values A and E are calculated to guide the pointing. It is difficult to determine the encoder values based on Equation (23). Thus, the encoder values A and E are determined using Equation (22). The guide value calculation is generated based on Equations (25–32):

$$(x_c, y_c, z_c)^T = R_{A\beta 1}^T R_\varphi R_c (x_g, y_g, z_g)^T \quad (25)$$

$$(x_p, y_p, z_p)^T = R_{B4}^T R_{B3}^T R_{B2}^T R_{A\beta 2} R_N R_{B1} R_E R_F R_{Mx} R_{Mz} (0, 1, 0)^T \quad (26)$$

Thus,

$$A_c = \arctan\left(\frac{x_c}{y_c}\right), E_c = \arcsin z_c \quad (27)$$

$$A + \Delta A_c = \arctan\left(\frac{x_p}{y_p}\right), E + \Delta E_c = \arcsin z_p \quad (28)$$

This results in Equation (29):

$$A = A_c - \Delta A_c, E = E_c - \Delta E_c \quad (29)$$

ΔA_c and ΔE_c are minimum values because each error term is a minimum value. Thus,

$$\begin{aligned} \tan(A + \Delta A_c) &= \frac{\sin(A + \Delta A_c)}{\cos(A + \Delta A_c)} \approx \frac{\sin A + \Delta A_c \cos A}{\cos A - \Delta A_c \sin A} \\ \sin(E + \Delta E_c) &\approx \sin E + \Delta E_c \cos E \end{aligned} \quad (30)$$

Based on Equations (26), (28), and (30), Equation (31) is obtained:

$$\begin{aligned} \Delta A_c &= \gamma_z \sec E - \eta \tan E - \xi_{B1} \sin E + \xi_{B2} \cos E + \xi_{B3} \sin A \cos A \tan E \\ &\quad + \xi_{B4} \cos^2 A \tan E + m_1 A / 2\pi + m_2 \sin A + m_3 \cos A \\ \Delta E_c &= E_{\beta 1} + \gamma_x + \delta_T \cot E + \xi_{B3} \cos^2 A - \xi_{B4} \sin A \cos A + n_1 E / 2\pi \\ &\quad + n_2 \sin E + n_3 \cos E \end{aligned} \quad (31)$$

Substituting Equation (29) into Equation (31) along with ΔA_c , ΔE_c and each error term being minimum values, yields Equation (32):

$$\begin{aligned} \Delta A_c &= \gamma_z \sec E_c - \eta \tan E_c - \xi_{B1} \sin E_c + \xi_{B2} \cos E_c + \xi_{B3} \sin A_c \cos A_c \tan E_c \\ &\quad + \xi_{B4} \cos^2 A_c \tan E_c + m_1 A_c / 2\pi + m_2 \sin A_c + m_3 \cos A_c \\ \Delta E_c &= E_{\beta 1} + \gamma_x + \delta_T \cot E_c + \xi_{B3} \cos^2 A_c - \xi_{B4} \sin A_c \cos A_c + n_1 E_c / 2\pi \\ &\quad + n_2 \sin E_c + n_3 \cos E_c \end{aligned} \quad (32)$$

The guide value calculation model is now complete. Equations (25), (27), (29), and (32) comprise the guide value calculation model. For Equation (25), $R_{A\beta 1}^T R_\varphi R_c$ is represented by



Fig. 5. The GOCT system.

Equation (33):

$$R_{A\beta 1}^T R_\varphi R_c = \begin{bmatrix} 1 & -\alpha_3 - A_{\beta 1} + \Delta P \sin R & -\alpha_1 - \Delta R + \Delta H \sin P \\ & -\Delta H \cos R \cos P & \\ \alpha_3 + A_{\beta 1} - \Delta P \sin R & 1 & \alpha_2 + \Delta P \cos R \\ +\Delta H \cos R \cos P & & +\Delta H \sin R \cos P \\ \alpha_1 + \Delta R - \Delta H \sin P & -\alpha_2 - \Delta P \cos R & 1 \\ & -\Delta H \sin R \cos P & \end{bmatrix} \quad (33)$$

The coupled error parameters are substituted into the calculation as a whole. Consequently, the coupled parameters do not influence the guide value calculation.

4. Experiment and Results

We developed a GOCT system (Fig. 5) to verify the proposed model. The results of our proposed model were compared to the results of the model in reference [13]. We refer to the model in reference [13] as Model A and our proposed model as Model B. We put the device system on a slope and rotated the whole device to change the attitude. This procedure simulated the motion platform. The GPS/INS integrated navigation system was installed on the GOCT system, which served as the attitude sensor for measuring the attitude of the device. The attitude angle errors respectively are 0.18mrad (1σ) in the yaw angle, 0.09mrad (1σ) in the pitch angle and the roll angle. The encoders of the azimuth axis and the elevation axis of the GOCT system have very high closed-loop guidance accuracy of 0.0005° (root-mean-square, RMS), which has a negligible effect on the pointing accuracy.

The method of tracking stars was applied in this experiment. Initially, the GOCT system tracked and measured a batch of stars in different attitudes. The GOCT system automatically recorded the position angles of the star in the Northeast celestial coordinate system (A_n, E_n), the attitudes of the device (H, P, R), and the encoder values (A, E) when the star was imaged at the center of the CCD. These measurement data were used in Model A and Model B to calculate the error

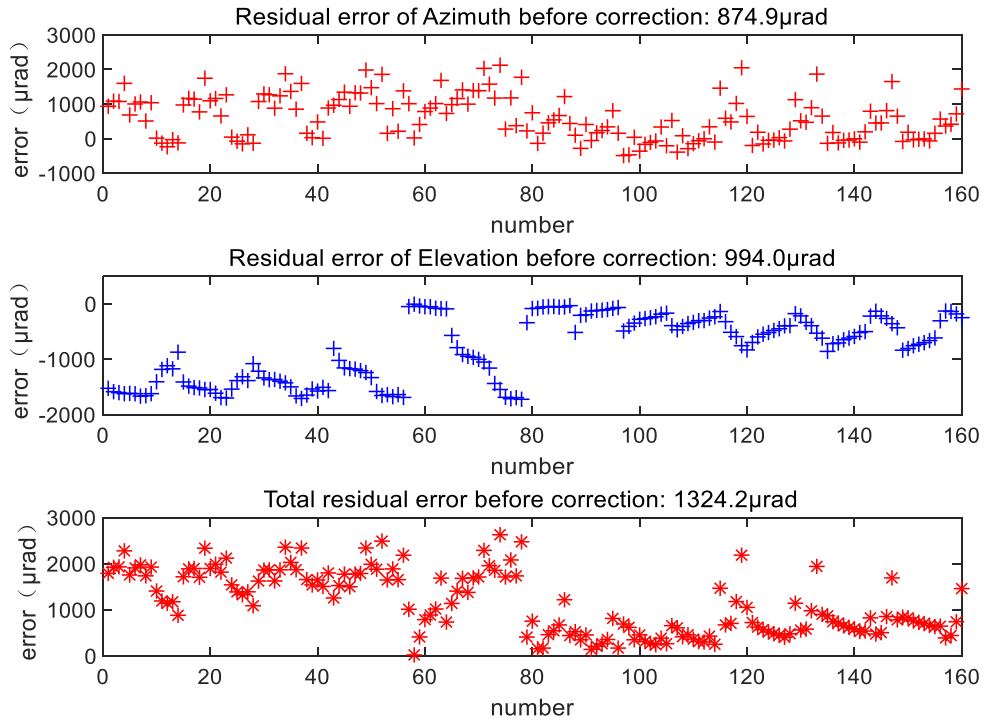


Fig. 6. The residual error before correction.

parameters and the modified residual errors. The residual error before correction is shown in Fig. 6. The residual error before correction is the initial pointing error of the system, which is determined by the manufacturing accuracy of the equipment and the measurement accuracy of the sensors. The modified residual errors after correction by Model A and Model B are shown in Fig. 7 and Fig. 8, respectively. Then, the GOCT system tracked and measured some stars in other different attitudes, and recorded the measurement data. These measurement data and the previously obtained error parameters were used to verify the open-loop pointing accuracy of Model A and Model B. The open-loop pointing errors of Model A and Model B are shown in Fig. 9 and Fig. 10, respectively. The total pointing error δ_{total} is given by Equation (34):

$$\delta_{total} = \sqrt{\delta_{azimuth}^2 + \delta_{elevation}^2} \quad (34)$$

where $\delta_{azimuth}$ (RMS) is the azimuth pointing error and $\delta_{elevation}$ (RMS) is the elevation pointing error.

All experimental data results are displayed in Fig. 6-10. Based on the data results displayed in Fig. 6 and Fig. 8, the modified residual error of Model B was $94.8 \mu\text{rad}$ compared to $1324.2 \mu\text{rad}$ for no correction. Based on the data results displayed in Fig. 7 and Fig. 8, the modified residual error of Model B was $94.8 \mu\text{rad}$ compared to $140.2 \mu\text{rad}$ of Model A. Based on the data results displayed in Fig. 9 and Fig. 10, the open-loop pointing error of Model B was $101.3 \mu\text{rad}$ compared to $150.4 \mu\text{rad}$ of Model A. The results of these comparisons demonstrate that our proposed model can greatly correct the initial pointing error of the GOCT under the same equipment accuracy conditions. In addition, since our proposed model considers more error sources and avoids the influence of error coupling, our proposed model has better pointing correction ability than the existing model. In short, the results of these experiments indicate that the proposed pointing model significantly improve the pointing accuracy of the GOCT on a motion platform.

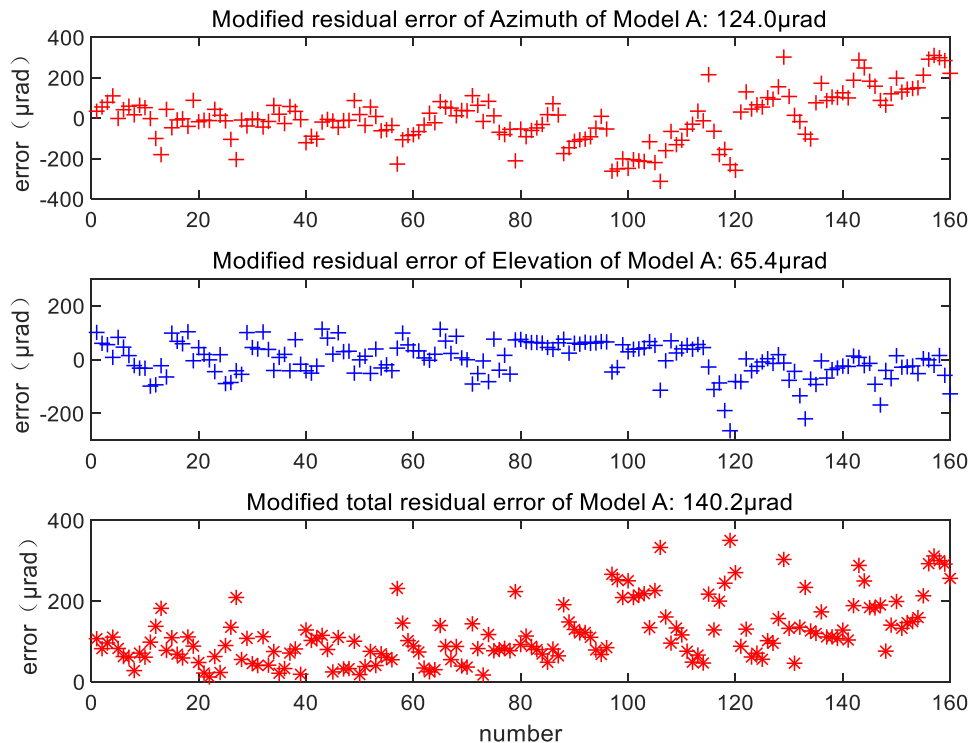


Fig. 7. The modified residual error after correction by Model A.

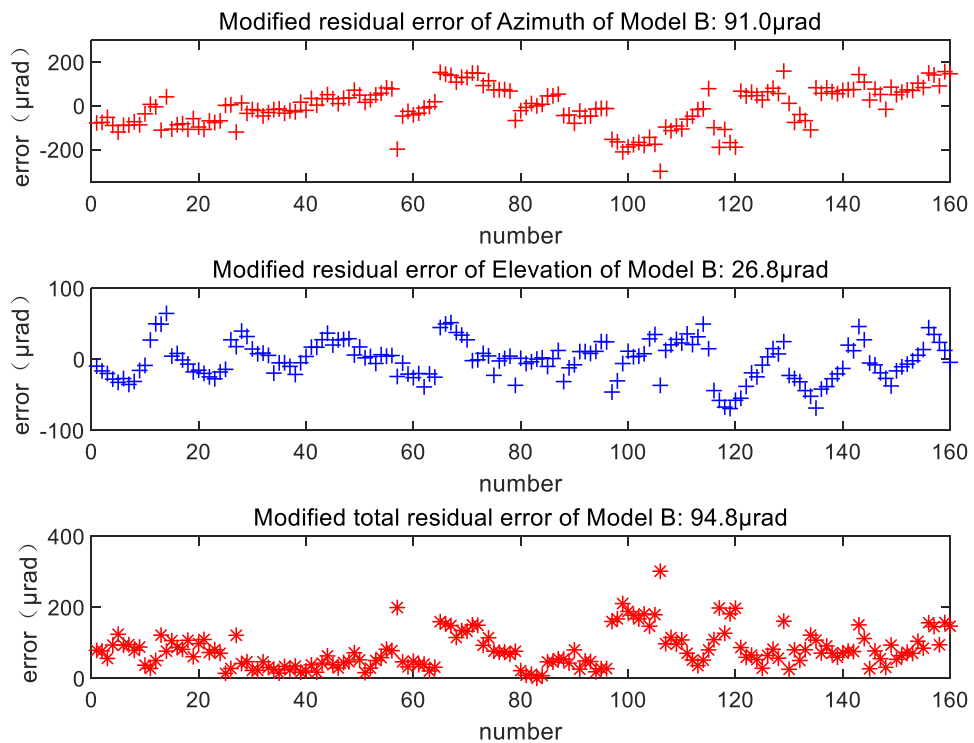


Fig. 8. The modified residual error after correction by Model B.

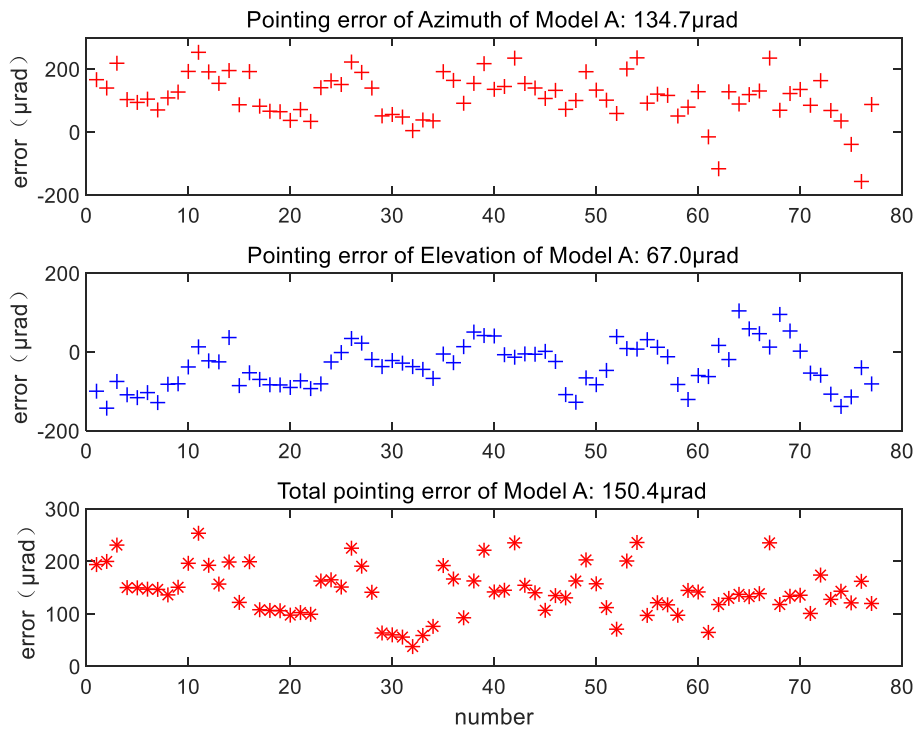


Fig. 9. The open-loop pointing error of Model A.

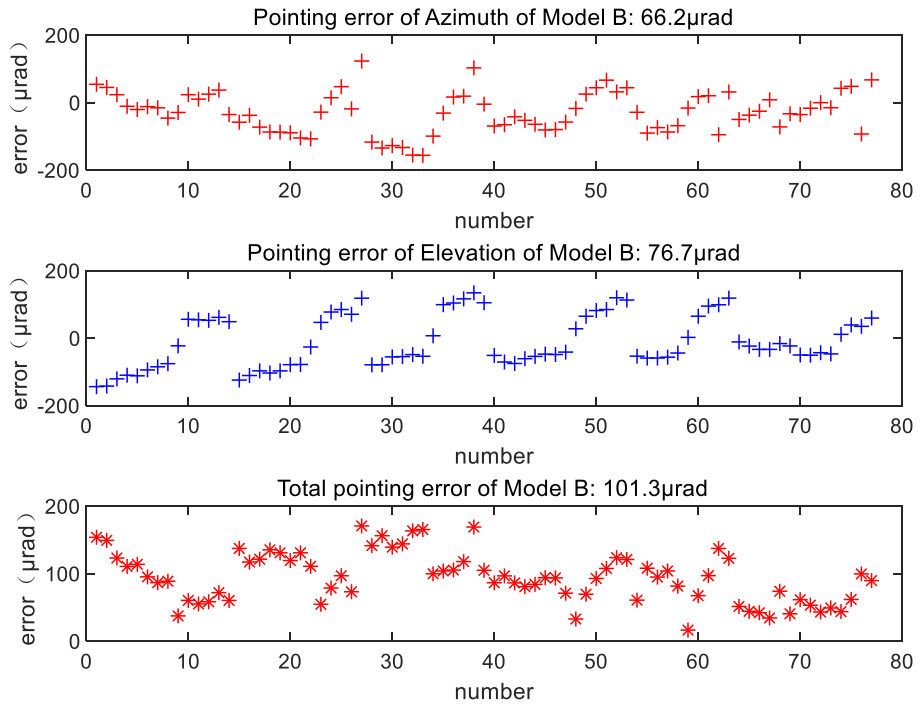


Fig. 10. The open-loop pointing error of Model B.

5. Conclusion

Attitude errors, installation errors, and geometric errors are the primary error sources that negatively affect the pointing accuracy of a GOCT on a motion platform. This study conducted detailed analysis and research on these error sources. The error matrix model of each error source was determined. Based on these error matrices, we derived a pointing model to improve the pointing accuracy of a GOCT. Our pointing model was comprised of an error parameter calculation model and a guide value calculation model. The error parameter calculation model simultaneously calculates all parameters, thus minimizing the coupling of parameter calculations. The guide value calculation model avoids the influence of coupled errors on the guide value calculation. The tracking star experiments verified the effectiveness of our proposed model. Compared with no correction, our proposed model reduced the modified residual error from $1324.2 \mu\text{rad}$ to $94.8 \mu\text{rad}$. In addition, compared with the existing model, our proposed model reduced the modified residual error from $140.2 \mu\text{rad}$ to $94.8 \mu\text{rad}$. Finally, compared with the existing model, our proposed model reduced the actual open-loop pointing error from $150.4 \mu\text{rad}$ to $101.3 \mu\text{rad}$. Thus, the pointing accuracy of a GOCT on a motion platform was significantly improved after correction by the proposed pointing model.

References

- [1] D. He *et al.*, "Acquisition technology for optical ground stations in satellite-ground quantum experiments," *Appl. Opt.*, vol. 57, no. 6, pp. 1351–1357, 2018.
- [2] L. Yan, Y. Huang, and Y. Zhang, "Using allan variance based semi-parameter model to calibrate pointing errors of Alt-az telescopes," *Appl. Sci.*, vol. 8, no. 4, Apr. 2018, Art. no. 614.
- [3] L. Huang, W. Ma, and J. Huang, "Modeling and calibration of pointing errors with alt-az telescope," *New Astron.*, vol. 47, pp. 105–110, 2016.
- [4] Q. Tang, X. Wang, and Q. Yang, "Static pointing error analysis of electro-optical detection systems," in *Proc. Inst. Mech. Engineers Part B J. Eng. Manufacture*, vol. 230, no. 3, pp. 539–600, Mar. 2016. doi: [10.1177/0954405414551107](https://doi.org/10.1177/0954405414551107).
- [5] J. W. Fisk, and A. K. Rue, "Confidence limits for the pointing error of gimbaled sensors," *IEEE Trans. Aerosp. Electron. Syst.*, vol. 2, no. 6, pp. 648–654, Nov. 2008.
- [6] S. Wu, L. Tan, S. Yu, and M. Jing, "Analysis and correction of axis error in periscope-type optical communication terminals," *Opt. Laser Technol.*, vol. 46, pp. 127–133, 2013.
- [7] J. M. Luck, "Mount model stability," in *Proc. 14th Int. Workshop on Laser Ranging Instrumentation*, 2004.
- [8] Y. Shim, S. D. Milner, and C. C. Davis, "A precise pointing technique for free space optical links and networks using kinematic GPS and local sensors," in *Free-Space Laser Communications VII*, San Diego, CA, USA, 2007, doi: [10.1117/12.739113](https://doi.org/10.1117/12.739113).
- [9] B. Epple, "Using a GPS-aided inertial system for coarse-pointing of free-space optical communication terminals," in *Proc. SPIE, Free-space Laser Communications VI*, vol. 6304, 2006, pp. U311–U320, doi: [10.1117/12.680502](https://doi.org/10.1117/12.680502).
- [10] R. Wu, X. Zhao, Y. Liu, and Y. Song, "Initial pointing technology of line of sight and its experimental testing in dynamic laser communication system," *IEEE Photon. J.*, vol. 11, no. 2, Apr. 2019, Art. no. 7903008.
- [11] Z. Xin, Y. Liu, and Y. Song, "Line of sight pointing technology for laser communication system between aircrafts," *Opt. Eng.*, vol. 56, no. 12, Dec. 2017, Art. no. 126107.
- [12] A. Shrestha, and M. Brechtelsbauer, "Transportable optical ground station for high-speed free-space laser communication," in *Proc. SPIE - Int. Soc. for Opt. Eng.*, vol. 8517, 2012, pp. 851706.851706.9.
- [13] D. He, *et al.*; "Shipborne Acquisition, Tracking, and Pointing Experimental Verifications towards Satellite-to-Sea laser communication," *Appl. Sci.*, vol. 9, no. 18, Sep. 2019, Art. no. 3940.
- [14] R. L. Meeks, "Improving telescope mechanical error estimates using pointing data," Ph.D. dissertation, Colorado State Univ., 2003.
- [15] H. Hong, X. Zhou, Z. Zhang, and D. Fan, "Modeling and calibration of pointing errors using a semi-parametric regression method with applications in inertially stabilized platforms," in *Proc. Inst. Mech. Engineers, Part B: J. Eng. Manufacture*, vol. 227, no. 10, pp. 1492–1503, 2013.
- [16] Q. Tang, "Analysis and research of pointing error of high precision multi-axis stabilized platform," Ph.D. dissertation, Tianjin Univ. China, 2014.